**Atmospheric
Chemistry
and Physics
Discussions**

Free troposphere as the dominant source of CCN in the Equatorial Pacific boundary layer: long-range transport and teleconnections

A. D. Clarke[1,2], S. Freitag[1], R. M. C. Simpson[2], J. G. Hudson[3], S. G. Howell[2], V. L. Brekhovskikh[2], T. Campos[4], V. N. Kapustin[2], and J. Zhou[2,*]

[1]Department of Meteorology, University of Hawaii at Manoa, Hawaii, USA
[2]Department of Oceanography, University of Hawaii at Manoa, Hawaii, USA
[3]Desert Research Institute, Nevada System of Higher Education, Reno, Nevada, USA
[4]National Center for Atmospheric Research, Boulder, Colorado, USA
[*]now at: Alstom Power Group AB, Sweden

Correspondence to: A. D. Clarke (tclarke@soest.hawaii.edu)

ACPD

13, 1279–1326, 2013

**CCN in the
Equatorial Pacific
boundary layer**

A. D. Clarke et al.

Title Page

Abstract | Introduction

Conclusions | References

Tables | Figures

◄◄ | ►►

◄ | ►

Back | Close

Full Screen / Esc

Printer-friendly Version

Interactive Discussion

Abstract

Airborne aerosol measurements in the central equatorial Pacific during PASE (Pacific Atmospheric Sulfur Experiment) revealed that cloud condensation nuclei (CCN) activated in marine boundary layer (MBL) clouds were dominated by entrainment from the free troposphere (FT). About 65 % entered at sizes effective as CCN in MBL clouds, while 25 % entered the MBL too small to activate but subsequently grew via gas to particle conversion. The remaining 10 % were inferred to be sea-salt aerosol; there was no discernable nucleation in the MBL. FT aerosols at low carbon monoxide (CO) mixing ratios (< 63 ppbv) were small and relatively volatile with a number mode around 30–40 nm dry diameter and tended to be associated with cloud outflow from distant deep convection (3000 km or more). Higher CO concentrations were commonly associated with trajectories from South America and the Amazon region (ca. 10 000 km away) and occurred in layers indicative of combustion sources partially scavenged by precipitation. These had number mode near 60–80 nm diameter with a large fraction already CCN.2 (those activated at 0.2 % supersaturation and representative of MBL clouds) before entrainment into the MBL. Flight averaged concentrations of CCN.2 were similar for measurements near the surface, below the inversion and above the inversion, confirming that subsidence of FT aerosol dominated MBL CCN.2. Concurrent flight-to-flight variations of CCN.2 at all altitudes below 3 km imply MBL CCN.2 concentrations were in quasi-equilibrium with the FT over a 2–3 day time scale. This extended FT transport over thousands of kilometers indicates teleconnections between MBL CCN and cloud-scavenged sources of both natural and/or residual combustion origin. The low aerosol scattering and mass in such layers results in poor detection by satellite and this source of CCN is not represented in most current models. The measurements confirm nucleation in the MBL was not evident during PASE and argue against the CLAW hypothesis being effective in this region during PASE.

1   Introduction

Lofting of both natural and combustion aerosol into the free troposphere (FT) followed by long range transport is well recognized and has been studied for decades. Volcanic emissions, dust, fires and large scale anthropogenic emissions have been traced thousands of kilometers. Substantial mass emissions of particles during these events often results in elevated light scattering detectable by satellites. Interest in such events has recently been driven by the need for greater understanding of the geochemical cycling of atmospheric constituents, the influence of emissions on atmospheric chemistry and the impact of anthropogenic emission on both aerosol optical depth (AOD), cloud condensation nuclei (CCN) and clouds. Modifications to atmospheric radiative processes, either as a result of changes in aerosol optical properties or changes in clouds through CCN (Twomey, 1974; Albrecht, 1989; Kaufman et al., 2002), are commonly referred to as the direct and indirect effects, respectively, and lead to potential impacts on climate. Recent studies have shown these effects are coupled (Hegg et al., 34; Andreae, 2009) and are manifested in regional differences over global scales linked primarily to combustion (Clarke and Kapustin, 2010).

Cloud pumping of species aloft is well recognized (Chatfield and Crutzen, 1990) and global transport has been a target of many airborne programs (e.g. Hoell et al., 1996). Concurrent scavenging of aerosol by deep convection can be effective and is often modeled as 100 % removal of particles but can be less effective at high aerosol concentrations (Jensen and Charlson, 1984). This reduction of aerosol mass and surface area in cloud outflow, in conjunction with cloud induced enhancements in actinic flux and reactive gas phase species and water vapor pumped aloft from the marine boundary layer (MBL) can produce conditions favorable for the formation of high numbers of small particles. Sulfuric acid aerosol nucleation initiated by late morning has been demonstrated to be an important global source of this "natural" aerosol (Clarke et al., 1998a). Convection in the equatorial Inter-Tropical Convergence Zone (ITCZ) has been linked to sulfuric acid aerosol produced from dimethyl sulfide (Clarke et al.,

CCN in the Equatorial Pacific boundary layer

A. D. Clarke et al.

Title Page

Abstract	Introduction
Conclusions	References
Tables	Figures

|◄   ►|

◄   ►

Back   Close

Full Screen / Esc

Printer-friendly Version

Interactive Discussion

1998b). These tend to dominate FT aerosol number in the Hadley circulation (Clarke and Kapustin, 2010). Following their subsidence into the MBL and growth through heterogeneous processes, some may reach sizes effective as CCN. Such natural aerosol, formed by low-temperature gas to particle conversion, is volatile in terms of both mass and number at temperatures below 360 °C.

Combustion-derived aerosols are often dominated by primary particles but may include secondary volatile and non-volatile aerosol. Generally, combustion aerosols contain non-volatile components (e.g. soot, black carbon, non-volatile organics) that remain after heating to 360 °C (Clarke and Kapustin, 2010; Thornberry et al., 2010). Hence, heating of the aerosol to 360 °C prior to measurement using a condensation nuclei (CN) counter can often provide a continuous index for combustion aerosol and larger aerosol even when contributions of non-volatile dust or sea-salt are low (though sufficiently large volatile aerosols may compromise this if they do not evaporate completely during the heating period). Volatile condensation nuclei are referred to here as CNvol and the non-volatile CN remaining at 360 °C we refer to here as CNhot. These properties and their links to gas phase measurements and CCN are used to characterize their relation to air masses and trajectories encountered over the equatorial Pacific. Here we demonstrate their entrainment into the MBL where they contribute to CCN.

2 Experiment location and features

The Pacific Atmospheric Sulfur Experiment (PASE) (Bandy et al., 2012) was conducted out of Christmas Is. (CI) in the equatorial Pacific during August–September, 2007. CI (157° W, 2° N) lies south of the ITCZ at this time of year. Because CI is located in easterly flow over a region with oceanic sources of dimethyl sulfide (DMS) it was expected to be a good region to study the natural marine sulfur cycle (Bandy et al., 1996; Faloona et al., 2009; Bandy et al., 2012) in a clean marine environment as the closest upwind continental sources are located about 10 000 km to the east in the northern part of South America (SA). The prevailing trade winds were easterly to south-easterly

with surface winds of 6–12 m s^{-1}. Trajectories in the lower FT have wind speeds of 8–14 m s^{-1} that can take ~ 10 days to reach CI after leaving SA.

PASE was a follow-up study of a ground based project on CI 1994 (Clarke et al., 1996). The influence of upwind sources was typically expected to be small in the MBL as this previous study found typical MBL aerosol lifetimes in this region were about 4 days or so (Clarke et al., 1996; Huebert et al., 1996). However, it became evident during PASE that fluctuations in carbon monoxide (CO) and ozone in the FT were associated with patchy transport of combustion derived gases and aerosol (Simpson, 2010). Such FT transport has previously been identified for ozone and has been linked to biomass burning over SA (Kim and Newchurch, 1996) known to be active at the time of PASE. Other measurements over the South Pacific have linked fluctuations in ozone and aerosol both from SA (Moore II et al., 2003) and the western Pacific (Browell et al., 2001).

Boundary layer particle concentrations throughout PASE were also higher than other clean MBL regions. Hudson and Noble (2009) reported average PASE CN concentrations of 379 cm^{-3} and CCN concentrations at 1 % supersaturation (S) of 301 cm^{-3} with the mean for each flight varying from 211 to 430 cm^{-3} and they noted frequent trajectories going back to SA. These are higher CCN than have typically been observed in maritime air masses such as during RICO (Rain in Cumulus Over the Ocean) in the Caribbean where mean boundary layer CN was 264 cm^{-3} and CCN at 1 % S was 106 cm^{-3} for 17 eight hour flights (Hudson and Noble, 2009).

Here we explore the relation of combustion and cloud outflow indicators to aerosol fluctuations and processes related to their link to CCN in the MBL. In order to compare PASE aerosol measurements to those made closer to the upwind sources we will also discuss some related observations from the VAMOS Ocean-Cloud-Atmosphere-Land Study Regional Experiment (VOCALS) based out of Chile in October/November, 2008. Both sampled air with elevated CO and ozone in trajectories leading back to northern South America.

3   Measurements and instrumentation

The Hawaii Group for Environmental Aerosol Research (HiGEAR) aerosol instrumentation focuses on size-resolved aerosol microphysics, chemistry, optics and radiative effects. Descriptions of the sampling inlet and most HiGEAR instruments can be found in (Clarke et al., 2004), the time-of-flight aerosol mass spectrometer (ToF-AMS), CO and ozone instruments are described elsewhere (Shank et al., 2012). Concurrently measured CCN spectra at various S are described in Hudson and Noble (2009) and Hudson et al. (2011). On several flights the CCN counter was sampling ambient air for less time than other measurements. Hence, some flight averages of CCN cover shorter periods than other data but we believe they remain representative. A brief summary of these measurements follows.

The ToF-AMS provided volatile ionic and organic aerosol chemistry for sizes between about 0.04 and 1 µm vacuum aerodynamic diameter (Shank et al., 2012); an Optical Particle Counter (OPC, LAS-X with custom electronics) covered sizes from 0.12 to 7.0 µm and included options for thermally resolved sizing at 40, 150, 360, and 400 °C. These sizes generally include most of the CCN activating at $S < 0.2$ %, those expected to be activated in MBL clouds and which correspond to aerosol sizes larger than the Hoppel minimum (Hoppel et al., 1994) discussed below. Two condensation nuclei counters (TSI Mod. 3010) were operated with condenser temperature 22 °C below the evaporator to measure total aerosol number density > 0.010 µm. One CN counter (hereafter referred to as CNcold) was without a heated inlet to measure ambient CN and the other was coupled to a heater operated at 360 °C to obtain non-volatile aerosol number > 0.010 µm (CNhot). CNvol is CNcold-CNhot. An ultrafine CN (UCN) counter (TSI Mod. 3025A) provided the number of particles > 0.003 µm; an Aerodynamic Particle Sizer (APS – TSI 3321) provided size spectra from 0.7 to 7.0 µm; light scattering extinction was provided by a 3-wavelength TSI integrating nephelometer (model 3563). A 1 µm size cut impactor was switched in to alternately provide total and submicrometer scattering. Two Differential Mobility Analyzers (DMAs) were used to obtain particle

size distributions. One was a TSI long DMA (LDMA, TSI 3081 with custom electronics) that measured particles between 0.1–0.5 µm in 60 s scans every 90 s. A radial DMA (rDMA; with custom electronics) scanned from 0.01–0.2 µm and was equipped with thermal denuders to measure size distributions before and after heating to 360 °C.

Both DMAs were equipped with grab samplers to ensure that entire scans (and sets of unheated/heated scans) used single air samples. We note that all size distributions and concentrations reported here are corrected to STP ($T = 25$ °C, 1013 mb) so that they are conserved over altitude changes and can be compared to mixing ratios such as CO.

CO and CNhot are employed here to provide gas and aerosol indicators to identify layers most likely to be influenced by combustion. The CO e-folding time in the tropics is near two months (Staudt et al., 2001) and CO is largely conserved during cloud processes. Over the transport time scales here (< 2 weeks) it provides a tracer for combustion influences in both the FT and MBL. In contrast, CNhot is scavenged in cloud but is expected to be stable in the FT.

Because CNhot is less commonly used, we show here the size-resolved influence of heating to 360 °C as measured by our rDMA. PASE spent little time in the FT and most of that was quick profiling up and down, so thermal DMA measurements were rare because they take several minutes so are usually done only on level legs. However, two examples are shown for research flight (RF) 8 in Fig. 1. This was a flight with layers of both elevated and low CO layers above the inversion.

Fig. 1a shows unheated (dashed) and heated (solid) distributions taken at 2250 m with CO at 80 ppb. Note the mono-modal unheated distribution with a peak near 0.09 µm. About 50 % of the number (area under plot) remain after heating. Many are shifted to much smaller sizes while the rest are volatilized. The distribution in Fig. 1b was taken at 1250 m altitude with low CO at 57 ppbv. The unheated distribution is bimodal with a dominant mode near 0.04 µm in diameter with a secondary mode above 0.1 µm. Less than 10 % remain after heating. Size resolved measurements for similar cases (not shown) indicate that many of these residual particles derive from

[ACPD](#)

13, 1279–1326, 2013

CCN in the Equatorial Pacific boundary layer

A. D. Clarke et al.

Full Screen / Esc

Printer-friendly Version

Interactive Discussion

Full Screen / Esc

Printer-friendly Version

Interactive Discussion

aerosol in the larger mode that has lost various amounts of volatile material (similar to Fig. 1a). The smaller size mode appears to completely volatilize (Fig. 1b), consistent with them nucleated from sulfuric acid in cloud outflow (Clarke et al., 1999a). These residual heated distributions are designated CNhot while the volatile mode are the CNvol (= CNcold − CNhot). Because these thermally resolved size distributions are infrequent, the rapid (1 Hz) measurement of CNhot and CNvol are used to provide insight into aerosol variability linked to size at the time scales required during profiles. The CNhot typically track with the larger size range > 0.08 μm and are better CCN at the low S characteristic of MBL clouds near CI.

4   Aerosol vertical profiles and transport

Although most flight time during PASE focused upon boundary layer measurements for flux studies, many flights included brief profiles into the FT. Two examples (Fig. 2) illustrate the flight patterns and gas and aerosol layers common for PASE. These were typically flown in a region approximately 500 km from CI where we would carry out stacked MBL legs interrupted occasionally with profiles through the inversion to about 3–4 km. Based upon observed CO values (Fig. 2a, b), we identify RF03 as a "low CO" and RF08 as "high CO" case. PASE flights 1–7 tended to have more low CO conditions and flights 8–14 tended to have higher CO (Simpson, 2010). However, as evident for RF08, both lower and higher CO values occur in layers at various altitudes. Such "layers" are commonly associated with increases in sulfur dioxide (SO_2), CCN, and CNhot (Fig. 2d, f, h), as expected for a combustion source. Approximately 100 FT profiles between the trade wind inversion (TWI) and 3 km or higher were done during the 14 PASE flights. The TWI height is calculated for each flight but was often located near 1300 m (Conley et al., 2011).

5 Natural aerosol from convective outflow

First we consider transport processes associated with the lower CO conditions exemplified by RF03 in Fig. 2. Such "clean" layers aloft are characterized by smaller more volatile particles observed in deep convective outflow (Clarke et al., 1999b) and commonly linked to trajectories reaching back to ITCZ convection. Most PASE flights were similar to those indicated in Fig. 2. One mission, RF04 (15 August), was dedicated to exploring cloud outflow in the ITCZ below 6 km. Our trajectories (see below) and winds suggested that this type of ITCZ outflow was a typical source of similar low CO layers commonly observed above CI.

Because of the distance to ITCZ convection, the limited flight time and the altitude constraints of the C-130 aircraft, this flight required a target-cloud that was accessible to the C-130 and active but detraining below 6 km. Such clouds were evident in less intense convection along the southern boundary of the ITCZ. This was identified by reviewing IR imagery the night before and selecting a cloud (Fig. 3a) with cloud top temperatures indicative of outflow near 5 km and predicted to advect within range (near 4.5° N, 157° W) the next day. This approach was similar to previously studied cloud-outflow altitudes referenced above but at lower altitudes than some of the more convective ITCZ clouds.

The selected cloud feature was higher than most of the surrounding trade wind cloud fields, like those in the linear along-wind cloud features evident in Fig. 3a. Numerous profiles were flown around this precipitating cloud near mid-day because earlier studies in Tasmania and the ITCZ, had revealed favorable photochemistry for nucleation of sulfuric acid existed by local noon (Clarke et al., 1998a). The initial RF04 profile to 6 km confirmed the major cloud outflow was between 4.0 and 4.5 km. Subsequent profiles to outflow altitudes included horizontal legs flown east, west and south of the cloud. CNhot are near 360 cm^{-3} at the surface but are highly scavenged in the outflow layer (Fig. 3b) while volatile CN (CNvol) are low near the surface but approach 3000 cm^{-3} in the outflow (Fig. 3c), which reflects their localized production.

Title Page

Abstract | Introduction

Conclusions | References

Tables | Figures

|◄ | ►|

◄ | ►

Back | Close

Full Screen / Esc

Printer-friendly Version

Interactive Discussion

Data for one such profile (Fig. 4) highlight key characteristics of the aerosol and related measurements. CN and UCN values (Fig. 4a) are similar from the surface to 3 km but UCN generally exceed CN values at higher altitudes reflecting the small nuclei in the 3–10 nm range associated with recent nucleation. Number concentrations peak in the outflow region near 4300 m and color coded number distributions on the right confirm their peak size near 20 nm with smaller sizes extending below the DMA detection limit of 10 nm. Largest sizes evident below 2 km are depleted in this layer consistent with the corresponding minimum in CNhot (about 20 cm^{-3}). As this convective cloud was rooted to updrafts from the MBL (evident visually), this indicates cloud scavenging of most CCN.

CO in the cloud outflow at 4200 m is 60 ppbv compared to 60–63 ppbv measured below 1000 m for the four profiles (Fig. 4b). CO varies between 54 and 60 ppbv in the intervening layers. CNhot in the outflow is near ~ 60 cm^{-3} compared to ~ 270 cm^{-3} below 1000 m and with values of 150 ± 30 cm^{-3} in the intervening layers. If we assume no mixing of BL air with the intervening layers during convection then this implies a lower limit of $\sim 80\%$ scavenging of the CNhot (and CCN) in the outflow. Any mixing of cloud scavenged air during convection with intervening layers will tend to increase CNhot and lower CO. The ~ 1–2 ppbv lower value for CO in the outflow compared to the BL could be due to mixing of about 20–30 % of the intervening layer air and this could contribute ~ 30–50 cm^{-3} additional CNhot (if none are scavenged) to the outflow. This would imply an increase in the estimated scavenged fraction of BL CNhot to $\sim 90\%$ or more. Hence, we consider 90 % to be a reasonable lower estimate for scavenging of BL CNhot and CCN for this cloud outflow near 4 km.

Ozone is higher immediately above and below the layer of elevated RH (ca 3500 m and 4500 m) which is consistent with generally higher ozone in the FT. The lower value for ozone at the outflow altitudes reflects the lofting and mixing of the MBL air with lower ozone. SO$_2$ also has a relative maximum in the outflow near 4000 m, probably related to both pumping aloft and conversion from DMS. This provides a source for sulfuric acid that leads to nucleation, as previously shown for the equatorial region

(Clarke et al., 1999b). Particles grow rapidly in these outflow layers until precursors are depleted, reaching sizes around 30–40 nm in this case. Because coagulation for these sizes is slow, these aged distributions can be stable until subsidence and entrainment brings them into contact with new sources.

6 Combustion aerosol from convective outflow

The low CO case above can be compared to RF 14 on 6 September 2007, one of the higher CO flights. In order to explore the relation of our in-situ measurements in these layers to potential source regions we merge our C-130 data into NOAA HYSPLIT (National Oceanic and Atmospheric Administration HYbrid Single Particle Lagrangian Integrated Trajectory) trajectory files (Draxler and Hess, 1997, 1998; Draxler, 1999). The back trajectories are generated through linear interpolation of trajectory fields for every 10 s and combined with our merged aircraft dataset, providing approximately 50 m resolution during vertical profiles. An example is shown in Fig. 5 for a complete profile from RF 14 where C-130 measurements are color scaled and mapped onto corresponding HYSPLIT trajectories. Figure 5a, shows trajectories colored by aircraft altitude above the inversion. Colors range from blue for lower altitudes near 1200 m to red at higher altitudes near 3200 m. Most elevated CO layers in the FT near CI were found within this range (see below). This 3-D visualization reveals that the air between 1200 m to 2200 m over CI had subsided during transport from SA. Above 2200 m air was associated with BL marine air that initially flowed from the SE into the ITCZ where it was lofted up to 6 km before subsiding to about 3 km near CI.

Figure 5b shows the same trajectories projected onto latitude and longitude and colored by time in days before arrival at the aircraft position. The circular features superimposed on the trajectories about 9 days back are sized in proportion to HYSPLIT estimated rainfall. These features follow the topography of the Andes mountains in SA toward the east and to a cluster of convective elements in the ITCZ to the north. Trajectories colored by measured CO (Fig. 5c) show highest CO for trajectories that passed

over SA within a few degrees of the equator between 60° W and 80° W. Lowest CO values are associated with those in the BL marine air transported to the ITCZ and lofted by convection.

The altitude vs. longitude projection of these profiles color coded with CO and CN-hot (Fig. 5d, e) reveal highest CO for trajectories encountered just above the inversion (ca. 1200 m) at CI. These subsided from altitudes east of the Andes near the equator about 9–11 days before. They are also enhanced in CNhot, consistent with non-volatile combustion derived CN. The marked variation in trajectory altitudes east of the Andes occurs in the region of deep convection indicated by the HYSPLIT rainfall and consistent with both the Andes topography followed by subsidence en-route to the CI study area. Near 3 km on the CI profile, the in-situ measurements are very different for the trajectories from the ITCZ where they were rapidly lifted in deep convection feed by BL flow from the SSE. These trajectories also have the lowest CO on the profile (and also low ozone not shown) consistent with clean aged BL air from the Southern Hemisphere. These trajectories represent clean air outflow from the ITCZ scavenged of larger aerosol (low CNhot) and enhanced in volatile nuclei (not shown), as discussed previously for Fig. 4. Although trajectory patterns differed from flight to flight, the interleaving of layers with combustion influence and clean layers were common and form the basis for the analysis that follows.

Although individual trajectories in excess of 10 days are often questionable, this equatorial region is commonly associated with stable and persistent winds after they leave SA. The example above shows the marked differences in air mass physiochemistry over the profile correspond to the altitudes showing marked difference in 12 day back trajectories. This would be expected and builds confidence in these trajectories for this region. Below we argue that convective activity associated with both of these distant air mass injections and subsequent transport constitute teleconnections to the BL aerosol and CCN over the central equatorial Pacific.

The Cloud Aerosol Lidar and Infrared Pathfinder Satellite Observations (CALIPSO; http://www-calipso.larc.nasa.gov/products/lidar/browse_images/production/) provide

additional support of the HYSPLIT clustering of trajectories over the equatorial Amazon region and evidence of convective lofting associated with precipitation. CALIPSO passes over this region can resolve convective cloud features and indicate inferred aerosol over altitude ranges Fig. 6 shows CALIPSO products near 65° W (8/27), and near 75° W (8/28) that match the time and location for the back trajectories shown in Fig. 5. The pass near 65° W shows a continental pollution 3–5 km thick (orange layer) extending continuously over two thousand kilometers. High clouds near 13 km and 7 km show frequent total attenuation (black) often associated with precipitation and scattered thunderstorms. The pass near 75° W and between 2° N and 6° S shows deep convection and heavy precipitation over the western Amazon basin near the Andes which is common at this time of year (Negri et al., 2000). Comparison with Fig. 5b shows that HYSPLIT trajectories indicate precipitation at this time. CALIPSO also reveals two aerosol layers both at the surface and aloft near equatorial clouds as well as above the Andes, consistent with the lifting, transport and expected scavenging of aerosol by this convection.

7 Stratification of clean and combustion influenced air masses

Clean and combustion influenced layers, as shown in Fig. 2 and exemplified by the distributions shown in Fig. 1, were evident on most flights. However, any given flight presents an incomplete picture regarding the possible influence of combustion layers and any link to MBL aerosol properties or CCN. This is because layers aloft are often a few hundred meters thick and are subsiding and being entrained at about 0.4–0.6 cm s^{-1} (Clarke et al., 1996; Huebert et al., 1996; Conley et al., 2009). Hence it takes on the order of a day for a layer to mix into the MBL. A combustion layer passing over the Andes near 5 km and subsiding at 0.5 ± 0.1 cm s^{-1} will take roughly 10 days to descend to the inversion (~ 1300 m) in the central Pacific. Variations in horizontal winds and subsidence mean that some layers encounter the inversion a day or two upwind or downwind of the CI region. Therefore, air we encountered in the PASE MBL

was probably influenced by previously entrained layers that are no longer present in the FT. Conversely, layers we encountered above the inversion will not have impacted the MBL prior to reaching CI. Consequently, combustion layers measured in the FT are seldom linked to same-day observations in the MBL. Moreover, the MBL reflects a mix of aerosol from prior advection and entrainment that has been exposed to additional sources of gas (e.g. DMS) and aerosol (e.g. sea-salt) all modulated by cloud processing. Hence, we focus our assessments on properties of aerosol transported in the FT.

8 Gas, aerosol and CCN relationships

Figure 7a shows the linear relation between CNhot and CO from a layer in the FT near 2 km on RF14 color coded by CCN measured at 0.2 % saturation (CCN.2). Other flights exhibit similar trends although slopes vary from case to case. This behavior is distinct from the volatile CN (CNvol) that commonly vary inversely with CO (e.g. Fig. 4). Figure 7b shows the relationship of CCN.2 to CNhot color-coded by flight number. This relation persists throughout PASE and has a tendency for higher values toward the end of PASE when CO tended to be higher. The relation of CNhot and CCN.2 differ somewhat for each flight but maintain a near 1 : 1 trend over the range of conditions during PASE. CNhot tend to exhibit larger sizes than most natural volatile aerosol and this accounts for their strong trend with CCN.2. Hence, we use the continuous CNhot measurement as an approximation of CCN.2 during periods of ambient data gaps of the CCN instrument.

Here we use CO to stratify all of the PASE profile data into cases with low CO, expected to represent clean and aged air masses, and those with higher CO, indicative of air more recently impacted by combustion sources. In order to select a threshold value for CO for separating data we use histograms of PASE CO as shown in Fig. 8. Here, we use boundary layer, BL, for the surface mixed layer in the MBL (0–600 m); buffer layer, BuL, for the MBL cloud layer (600–1300 m); lower FT for measurements made

between 1300–3000 m and upper FT for observations above 3000 m. The different frequency scales show the vast majority of time was spent below the trade wind inversion with far fewer measurements in the FT. As we will want to compare excursions in particle behavior to excursions in combustion derived CO, we assume here that 50 ppbv represents an effective equatorial Pacific background for CO free of combustion influence. We later use CO-50 ppbv as a reference for deviations from clean air conditions in this region.

Clear distinctions are evident in each of the histograms with a cluster of high frequencies of occurrence of CO below about 63 ppbv (blue histograms) at all altitudes and a broader range of values above that. The largest range of concentrations is evident in the lower FT, where distinct air mass types can persist with limited mixing. Values above 63 ppbv (red histograms) are least common above 3 km. The lowest CO has been pumped aloft in the ITCZ and aged longer. Assuming a lifetime of 50 days in the tropics (Staudt et al., 2001), FT air at 58 ppbv would drop to about 53 ppbv after about 4.5 days aloft. This could be shorter in regions of elevated hydroxyl radicals (OH), as expected around deep convective clouds. CO histograms in the BuL reflect the mixing of CO concentrations in the BL with air in the lower FT. The narrowest range of values are in the BL, as expected for an evolving mix of higher and lower values from aloft.

We arbitrarily use CO at 63 ppbv to stratify various data into "low CO" (blue) and "high CO" (red) categories and show profiles for all PASE flights in Fig. 9. When CNhot and CNvol (Fig. 9b, c) are stratified with these criteria the higher CO cases tend to have higher CNhot and lower CNvol than those with CO < 63 ppbv both in the FT and in the MBL. Nominal MBL CCN (Fig. 9d), the number of particles larger than 80 nm (N_{80}) obtained from integrating measured size distributions larger than the Hoppel minimum, are also greater for the higher CO cases. Submicrometer light scattering, dominated by optically active sizes between 0.1 and 1.0 μm, is elevated in air masses above the mixed layer having higher CO (Fig. 9g), as also demonstrated in Fig. 7c.

It is interesting to compare the various number profiles in Fig. 9b–f: CNhot, CNvol, N_{80}, CCN.2 and CCN.2-CCN.04 (CCN.04 are those activated at 0.04 % supersaturation). CNvol are distinct in that they increase steadily with altitude while the others all decrease or are variable. CNvol also show little difference with CO, indicating that these smaller volatile aerosol are associated with sources aloft only weakly related to variations in CO. CNhot tend to be higher near the surface and decrease aloft with a layered character. Large excursions are evident at a given altitude that correspond to sequential data from level legs, indicating marked horizontal variability. CNhot are also typically much higher when CO is elevated. There are fewer measurements of N_{80} but these are quite similar to CCN.2 in their decrease with altitude but are slightly higher in MBL concentrations. This suggests that typical MBL cloud S that establishes the Hoppel minimum near 80 nm is slightly above about 0.2 %. Higher CO aloft is generally associated with higher values for both. Because CCN larger than about 200 nm are activated at low S near 0.04 %, we can subtract these CCN.04 from those measured at 0.2 % S to examine sizes that dominate CCN number typical of MBL clouds (Fig. 9f). This crude approach effectively removes the contribution of largest aerosol (particularly larger sea-salt present below the inversion). Aloft there is little difference from CCN.2 (Fig. 9e) as there are relatively few larger aerosol there. However, in the MBL the CCN.2-CCN.04 are lower than the CCN.2 and show less variability.

In spite of more limited CCN measurements on the FT profiles the CCN0.2-CCN0.04 are greater in the presence of enhanced CO (Fig. 9f). Less difference is evident in the BL but mean values are only 20 cm^{-3} higher than those aloft. In the MBL values are about 125 cm^{-3} compared to about 180 cm^{-3} for CCN.2 indicating an increase of about 55 cm^{-3} above FT values arising due to a combination of sea-salt production and or aerosol growth into larger sizes above ~ 200 nm. Lowest values aloft for N_{80}, CNhot and CCN.2 are in the 30–50 cm^{-3} range and most common for lowest CO. This is consistent with values previously discussed in conjunction with cloud outflow (Fig. 4) suggesting that it accounts for the lower values of CCN.2 present in the FT in this region.

Title Page

Abstract | Introduction

Conclusions | References

Tables | Figures

◄◄ | ►►

◄ | ►

Back | Close

Full Screen / Esc

Printer-friendly Version

Interactive Discussion

It is also interesting to note that elevated CO is associated with higher winds during PASE (Fig. 9h) and more rapid transport. These higher winds may result in more effective ventilation of the surface ocean (Yang et al., 2011) leading to higher atmospheric DMS concentrations (Fig. 9i) and potentially faster aerosol growth.

The CO stratification above is also applied to the combined size distributions measured by the DMAs, OPC and APS in Fig. 10. These generally represent merges of distributions collected over approximately 1 min. The stratified size distribution profiles (Fig. 10a–d) represent means over the entire PASE campaign and can be viewed as that expected for a PASE profile if low CO were present at all altitudes (Fig. 10a, c) compared with a profile if CO were elevated at all altitudes (Fig. 10b, d). The dashed vertical reference line near 80 nm is included to reveal differences in sizes based on this CO stratification. This value is chosen to visually separate sizes that are expected to be CCN.2 (i.e. > 80 nm) in typical PASE MBL clouds, as evident by the pronounced Hoppel minimum in the BL.

Above 1500 m the number of particles larger than 80 nm (Fig. 10a, b) is significantly higher for the high CO cases. The number size distribution peaks are also shifted to larger sizes by a factor of about 1.6, which corresponds to about 4 times as much mass per particle. This difference is more evident in the particle surface area plots for the FT (Fig. 10c, d). Below the inversion growth in this size range is linked to sulfate production from DMS. DMS is highest in the BL and negligible in the FT (Fig. 9i) with active conversion in the BuL (Simpson, 2010).

These differences are more evident when separately averaging all measured clean (Fig. 10e) and combustion-influenced (Fig. 10f) PASE number size distributions stratified over selected altitude ranges. These ranges are chosen to reflect the mean mixed layer (0–600 m), the BuL (600–1300 m), the layer just above the inversion (typically found near 1300–1700 m), and the adjacent FT ($\sim$ 1700–2500 m) where CO layers were most common (Fig. 9a). The FT distributions (black lines) with higher CO have a number mode above 60 nm (Fig. 10f) while the lower CO case peaks at 40 nm (Fig. 10e).

CCN in the Equatorial Pacific boundary layer

A. D. Clarke et al.

For the clean case at slightly lower altitudes just above the inversion (1300–1700 m), concentrations compared to the FT layer are the same near the Hoppel minimum, greater at large sizes and lower at small sizes but total number (area under these two curves) is approximately the same. Below the inversion in the BuL (cloud layer) the Hoppel minimum is prominent near 80 nm (black dashed line) and concentrations exceed those in the FT for sizes greater than this minimum but are less for smaller sizes. The two modes associated with the Hoppel minimum are larger at the lowest altitude (BL) than the BuL, which suggests a net growth of smaller sizes through the Hoppel minimum.

The general shape of the combustion-influenced distributions (Fig. 10f) reveals similarity of BL and BuL distributions and a greater fraction appear to have grown through the Hoppel minimum, indicative of cloud processing. In the MBL, the relative reduction in concentrations of sizes below the Hoppel minimum, relative to FT values, is a large fraction of the relative increase in concentrations of particles larger than the Hoppel minimum. These plots also demonstrate that there is a smaller fraction of aerosol that did not act as CCN in the MBL when CO is higher. This is consistent with more FT aerosol being larger and more likely to be CCN compared to the low CO cases. However, it is important to note that the BL distributions represent the net effect of entrainment that took place upwind of measured profiles while the FT data are yet to be entrained and will only influence the MBL over the next several days. We have also not yet accounted for sea-salt present in the MBL (Hudson et al., 2011) or the observations of vertical mixing near the end of PASE when winds and CO values were generally higher and when boundary layer rolls were more prevalent.

We note that size distributions in Fig. 10 involve cloud outflow mixing with preexisting aged FT aerosol probably derived from similar processes in the past. Hence, both groupings include contributions from preexisting FT aerosol so they are less well defined than distributions for individual cases (Fig. 1).

For a steady state inversion height, growth in the MBL will reflect sulfate conversion from DMS during the residence time established by the balance between entrainment

and divergence. Growth is expected to be greater for activated sizes than interstitial sizes as their in-cloud surface areas will be far greater. Moreover, in-cloud aqueous phase chemistry can add more mass than in clear air (Simpson, 2010).

9 Entrainment and regional CCN variability

The discussion above provides a context for looking at the variations in CCN during PASE. A comparison of the sizes above and below cloud (Fig. 10) reveals the development of the Hoppel minimum near 80 nm, which is approximately the minimum diameter for an ammonium bisulfate particle to activate at 0.2 % S, typical in trade wind cumulus (Cu). This is the motivation for our use of CCN.2 as a representative measure of actual CCN activated in this region. However, the width of this minimum indicates higher S near 0.3 % or so must have activated some dry sizes as small as 50 nm (grey dashed lines in Fig. 10). Figure 10e, f indicates the typical diameter increases for the larger activated sizes near 150 nm is about a factor of two while for the unactivated mode near 40 nm it is closer to a factor of 1.4 (CO > 63) to 1.6 (CO < 63). This indicates that larger activated sizes from the FT have increased their mass in the MBL by roughly a factor of 8 while the unactivated sizes have increased their mass about a factor of 3 (CO > 63) to 4 (CO < 63). Because the latter growth occurs on much smaller sizes this mass represents only about 5 % of the total mass added to the aerosol.

We consider here the flight-by-flight variability in the altitude resolved CO, CNhot, CNvol, CCN.2 and CCN.04. The difference of the latter two excludes the largest of the CCN activated at an S of 0.04 % corresponding to sizes above about 240 nm for ammonium bisulfate and about 190 nm for sea-salt. In Fig. 11a we show measured CO for each PASE flight averaged over three altitude ranges: BL (0–600 m), BuL (600 m to the inversion) and above inversion (inversion to ca. 3 km). In spite of less data in the BuL and least in the FT, there is enough for representative comparisons over all 3 altitudes. Cases with elevated CO aloft are more evident in the second half of the

experiment (Simpson, 2010) and CO in the MBL tends to be higher than the FT in early flights.

In panel 11b (and Fig. 9b) CNhot in the FT tend to be lower than in the BuL and BL. This is due to both addition of non-volatile sea-salt at the surface but also the growth from smaller to larger sizes that can lead to reduced volatile number (Fig. 1). The CNvol in Fig. 11c are clearly higher in the FT but rapidly decrease in the BuL and generally have lowest values in the BL. This rapid decrease indicates effective removal of the smaller CNvol in the BuL via unresolved cloud related processes. Variations in CCN.2 in panel 11d show both absolute and relative concentrations are similar to variations in CNhot except for the anomalous ITCZ cloud flight, RF04. Panel 11e demonstrates CCN.04 for each flight are a small fraction of the CCN.2 and their concentrations in the FT are less than the BL or Bul both because there is sea-salt produced in the BL and because growth to larger sizes is most active below the inversion. Their relative contribution is largest in the BuL on the more polluted flights such as 8 and 12–14 (also where CO is a maximum in the BuL) and indicates active entrainment.

In order to better reveal the trends for the smaller CCN.2 that dominate CCN in MBL clouds we subtract the average CCN.04 from the average CCN.2 at each altitude to get the plot in Fig. 11f. The number of data points in these averages varies from flight to flight because each flight varied in the amount of time at each altitude range (Fig. 2) and because the CCN counter was not always making ambient measurements for the entire flight. Nevertheless, these CCN from the FT contribute about 80 % (±20 %) to similar sizes that dominate CCN in the MBL (i.e. CCN0.2-CCN0.4). This percentage would trend larger if we included the contributions from sizes below 80 nm in the FT that grew through the Hoppel minimum when activated by higher than average S (e.g. between grey and black dashed lines in Fig. 10). Once activated in cloud (perhaps during the entrainment process) these can add mass heterogeneously and, in subsequent cloud cycles, will be more favored to activate at a lower S. These observations confirm most CCN in MBL clouds over CI were derived from the FT via entrainment.

Moreover, the variations between these concentrations (Fig. 11f) at different altitudes on a given flight are generally smaller than the intra-flight variations. Because PASE flights were typically separated by two or three days, this shows that synoptic scale variations in CCN between flights at all altitudes exceed typical differences between the MBL and FT concentrations on a given flight. This indicates MBL CCN.2 must respond on a similar 2–3 day time scale to variations in FT concentrations and implies that these concentrations are in pseudo-equilibrium.

These features are also expressed in the campaign mean values shown in Table 1. As in Fig. 11, the data have been averaged over all flights for values near the surface (BL), below the inversion (BuL) and above the inversion (FT < 3 km). Here, measured CCN activated 0.4 % S (CCN.4) has also been included to provide a sense of the sensitivity of the number of CCN to actual supersaturations between 0.2–0.4 %. The last two columns also include the means for the BL and BuL, after subtracting values from above the inversion. CNhot are substantial aloft but increase toward the surface reflecting both the contributions of non-volatile sea salt aerosol (SSA) and the increase in size from uptake of sulfate that tends to leave some residual mass at smallest sizes when heated (see discussion below). This growth can effectively convert some CNvol to larger sizes that may be detected as CNhot.

The total CN averaged over the PASE campaign are 438, 429 and 533 cm^{-3} for surface, below and above the inversion respectively. Because nucleation in the MBL was not evident and as non-volatile SSA will contribute to CNhot, then a marked reduction in the CNvol entrained into the MBL indicates rapid loss of smaller volatile particles in the BuL, perhaps associated with the cloud-related entrainment process. Size distributions of SSA larger than about 750 nm include about 2.5 cm^{-3} in the BL and about 1.2 cm^{-3} in BuL. Enhanced MBL surface area below $\sim$ 1500 m (Fig. 10) is primarily due to seasalt and can be compared to dry SSA size distributions established for breaking waves (Clarke et al., 2006). That data showed about 8 % of the freshly produced SSA number were larger than 750 nm and 50 % ($\sim$ a factor of 6 more) were larger than about 80 nm. Assuming the shape of the SSA distribution is the same for PASE, scaling by $\sim$ 6 times

the observed concentration above 750 nm implies SSA on PASE should include about 15 cm^{-3} larger than 80 nm (nominal CCN.2) in the lower BL and about 15 cm^{-3} (total) or 8 cm^{-3} larger than 80 nm in the BuL.

Subtracting these estimated SSA from the measured CCN.2 we are left with the sub-750 nm non-SSA CCN.2 as 177 cm^{-3} (192 cm^{-3} minus 15 cm^{-3}) in the BL (similar to Hudson et al., 2011) and 174 cm^{-3} (182 cm^{-3} minus 8 cm^{-3}) in BuL. Because the mean above-inversion CCN.2 concentration is around 125 cm^{-3} this suggests there are about 50 cm^{-3} more non-SSA CCN.2 in the BuL and BL than aloft. These estimates imply that increases in both CCN and CNhot below the inversion are primarily a result of growth through the Hoppel minimum to larger sizes, as indicated in Fig. 10b.

10   Entrainment scales and mixing into the MBL

The above observations confirm that patchy layers of enhanced combustion aerosol several hundred meters thick can subside as rivers of pollution that ultimately encounter the inversion and become entrained into the MBL. Consequently, we expect some gradients of CO and aerosol in the MBL to vary not only due to the differences in spatial scales, concentration and thickness of such layers but also the wind shear, turbulence and cloud activity etc. Investigating MBL aerosol gradients within our sampling strategy was not planned but boundary layer variations in CO and aerosol properties were often evident (e.g. Fig. 2).

In RF05 we flew our sample pattern across a BL gradient that persisted over 6 h and showed corresponding variations of CO with CCN.2 and aerosol features (Fig. 12a). The only profile that day into the FT around 18:00 UTC also reveals enhanced CO aloft that varies with CCN.2 (Fig. 12b). For this profile, MBL CO was well mixed up to about 800 m where it increased to about 59 ppbv. This value held up to the inversion near 1340 m (solid grey line) above which it increased to 63 ppbv. Measurements from a later profile (Fig. 12c) around 00:30 UTC and located about 50 km east of the first profile reveal enhanced CO and CCN.2 present at lower altitudes.

Wind directions varied systematically from about 80–100° with a period of about 90 min and wind speeds were 8–11 m s^{-1} in the MBL and about 14 m s^{-1} above the inversion. The gradient in CO over the Vs persisted over flight duration but trended lower by about 1 ppbv as the air advected through the V pattern (not shown). Since wind direction remains approximately constant, this gradient and these profiles demonstrate active entrainment of air with elevated CO through the inversion and into the BuL and BL. However, given the presence of both velocity and directional wind shear across the inversion, entrainment rates for patchy FT pollution layers are difficult to quantify.

The size distribution (not shown) from the 2000 m layer of elevated CO (Fig. 12b) was shifted to the larger sizes characteristic of "high CO" distributions as shown in Figs. 1 and 10b. Here about half the number are larger than 80 nm and will be immediately CCN.2 in the MBL. There was also enhanced volume (mass) evident around a mode diameter of 0.15 µm in this layer. Even so, this is only about one third the mass present for this mode in the MBL. Consequently, even though this combustion aerosol aloft can contribute to the flux of sulfate mass into the MBL (Simpson, 2010) the associated mixing and divergence would actually reduce (dilute) the MBL mass concentrations. In contrast, because the associated CN (not shown) and CCN.2 number concentrations are greater at 2000 m (Fig. 12b) than in the MBL, entrainment will lead to a concurrent increase of CN and CCN.2 concentrations in the MBL.

The common trend evident in CNhot and CCN.2 with CO (Fig. 12a) indicate entrainment is influencing all three observations over a 100 km scale in the BL. In this case, CCN.2 increases from about 170 cm^{-3} to 225 cm^{-3} or about 30 % as CO increases from 58 to 61 ppbv, implying active entrainment of FT air. If the gradient in aerosol was driven by precipitation scavenging (very low in this region) we would not expect to see a gradient in CO as it would be conserved for this process.

When CO remains in the 60–61 ppbv range the AMS sulfate (Fig. 12a) increases from about 4 to 5 µg m^{-3}, far more than corresponding changes in CCN.2 and CNhot. This may result from the continued addition of sulfate mass to the entrained CCN.2 after they reaches their peak concentration. This apparent addition occurs in

the region where greatest cloud density was evident in the BuL based upon measured reductions in downwelling UV radiance and in-flight video observations (not shown). We speculate that in-cloud processes may be responsible for this relative increase in mass (Simpson, 2010). Also note that all CO values lie just below our threshold of
5   63 ppbv for " low CO ", indicating that even this low value does not ensure combustion aerosol will be excluded. We note that Moderate Resolution Imaging Spectroradiometer (MODIS; http://earthdata.nasa.gov/data/nrt-data/rapid-response) imagery (not shown) commonly showed similar streets of clouds adjacent to cloud free regions along the wind that may travel together for several days. These differences are a reminder that
10   sampling a representative aerosol, even in the most remote oceanic regions, needs to be considered carefully and with attention to cloud features.

11   Discussion and conclusions

Repeated flight patterns in the equatorial Pacific flown during PASE revealed the re-lation between FT and MBL aerosol in the equatorial Pacific and its variability. Data
15   characterized by CO greater and less than 63 ppbv was used to stratify aerosol layers associated with more natural processes in this region and those impacted by combus-tion. The resulting mean profiles in Fig. 10 and the altitude averaged distributions are illustrative but the averaging tends to broaden the modes and mask variability present on a given profile, as evident in Fig. 1. Even so, the areas (proportional to total number)
20   under all of these distributions in Fig. 10e, f are clearly similar, indicating that number is largely conserved through subsidence and entrainment. This is also indicative of weak in-cloud coagulation and removal, consistent with the low rainfall in this region. The negligible contributions to sizes below 20 nm in the MBL and the presence of smaller sizes in the FT than the MBL confirm that nucleation in the MBL is not a significant
25   contribution to aerosol number. The mean profiles for both lower and higher CO on PASE (Fig. 9b, f) demonstrate that the MBL number population, other than sea-salt, is directly linked to the FT distribution. This confirms most of the population is typically

resupplied through entrainment from the FT rather than nucleation and growth in the MBL.

The case study of ITCZ convection on RF04 demonstrated scavenging of boundary layer marine aerosol and CCN was about 90 % effective and nucleation was active in this outflow region. This example is taken to represent processes in ITCZ regions that influence scavenged layers with elevated nuclei and low CO encountered in the FT near CI.

The mean FT size distribution above the inversion for higher CO in Fig. 10f has a mode diameter about a factor of two smaller (about an order of magnitude less mass per particle) than observed in combustion outflow near SA using these same instruments (Moore II et al., 2003) and these are far below sizes reported for Amazon biomass burning at the surface (Rissler et al., 2006; Soto-García et al., 2011). Deep convection over the Amazon has been found to loft aerosol to 10 km while scavenging about 90 % of the accumulation mode before advection out over the Pacific (Andreae et al., 2001). Surface studies in the Venezuelan Andes near 4800 m also argue for active scavenging of BL aerosol lofted into the FT (Schmeissner et al., 2011). Typically the larger sizes are those most effectively scavenged. Even so, under high smoke conditions, suppression of precipitation can allow smoke to be lofted through clouds to altitudes above 5 km without removal (Andreae et al., 2004).

In order to identify which mechanism is most consistent with PASE data, we consider excursions in CO above a nominal background of 50 ppbv as a conservative gas-phase tracer to compare with aerosol variations. We then compare the ratio of aerosol to CO-50 on PASE compared to similar ratios nearer sources. We consider the relation of aerosol light scattering to CO and the relation of CNhot to CO as we have made measurements of both near sources in South America. Using the above-inversion flight averages for light scattering (not shown) we obtained a mean slope of scattering (dominated by accumulation mode aerosol) vs. CO of 0.15 Mm^{-1} ppbv^{-1} with an R^2 of 0.85 (excluding RF06). This is about 10 to 20 % of the slope we have obtained on various experiments (Clarke and Kapustin, 2010) near combustion sources. Our recent

unpublished data for biomass burning aerosol off the coast of South America during VOCALS have values near $1 \, \text{Mm}^{-1} \text{ppbv}^{-1}$. If we accounted for the slow destruction of CO during transport, the mean slope for PASE would be even lower. Hence, our data is consistent with most CO layers above the inversion being preferentially scavenged of most aerosol during deep convection near their source (e.g. Fig. 5b).

A similar conclusion is reached if we compare the relation of CNhot to CO (e.g. Fig. 7a). These show about a factor of 4–5 reduction in the ratio of CNhot to CO near sources and consistent with similar conclusions for high altitude combustion plumes off SA based on comparisons of CNhot with ozone (Moore II et al., 2003). Because the accumulation mode dominates light scattering and because it is typically greatly reduced in these plumes they are not readily detected by satellite. For example, the strongest scattering layers on PASE were about $10 \, \text{Mm}^{-1}$ (Fig. 7c) and, if distributed over a typical 300 m layer, the contributions to AOD would be only 0.03 and with most other layers being far less. Nor are residual CCN from prior scavenging well represented in most current models. However, these observations and the significance of combustion derived aerosol in the FT and its impact on MBL CCN confirm their importance to global models (Merikanto et al., 2009).

These scavenged combustion layers over the central Pacific contribute effective CCN.2 when entrained into the MBL. Combustion derived aerosol are typically larger sizes and differ in composition from the aerosol nucleated in ITCZ outflow and dominated by sulfuric acid (Clarke et al., 1999b). Measurements in combustion aerosol over the Amazon show that organic carbon (OC) dominates aerosol mass. Over half of it is volatile upon heating to $360\,°C$ and largely water soluble (Soto-García et al., 2011). Even greater OC fractions were observed in the wet season (Gunthe et al., 2009) and both periods reveal larger OC fraction (up to 90 %) in the Aitken size range. These were argued to be effective CCN but with a reduced hygroscopicity parameter, κ, of 0.1 at 50 nm compared to 0.2 at 200 nm. Although evidence of nucleation has been seen at altitude above the Amazon, the low SO_2 and sulfuric acid production cannot explain the observed rate of growth of these aerosol and biogenic volatile organic carbon probably

Full Screen / Esc

Printer-friendly Version

Interactive Discussion

Full Screen / Esc

Printer-friendly Version

Interactive Discussion

plays a role (Martin et al., 2010) and references therein. Consequently, it is likely that the cloud-scavenged combustion aerosol seen aloft during PASE is enhanced in OC until entrained into the MBL where gas to particle conversion will increase the relative sulfate fraction.

As mentioned earlier, nuclei formed in ITCZ outflow are mostly volatile and consistent with nucleation from measured sulfuric acid. Our flight averaged data for volatile CN in Fig. 11 (and Table 1) shows these smaller nuclei are preferentially depleted when entrained into the MBL compared to the larger sizes more effective as CCN. Even though these outflow nuclei are a major source of FT aerosol number they appear to contribute far less to MBL CCN.2 than those linked to higher CO from long range transport, at least during the biomass burning season. This also indicates that unless an airmass is well scavenged by deep convection (as in the RF04 outflow example) and precursors are introduced into an FT with low preexisting aerosol, then nucleation and subsequent growth to larger sizes may be suppressed (Clarke, 1993; Merikanto et al., 2009). Enhanced scavenging of these smaller sizes have been observed and modeled to increase by an order of magnitude as sizes decrease from about 50 to 10 nm diameter in response to various processes (Andronache et al., 2006) acting on aerosol mixed up into precipitating cloud. However, the Andronache et al. study did not consider interaction of cloud droplets with entrained dry FT/BuL air, as occurring here during PASE.

We argue from Table 1 that a mean CCN.2 of 190 cm^{-3} in the MBL during PASE, approximately 125 cm^{-3} were entrained as CCN.2 from the FT and about 15 cm^{-3} were produced as SSA. We also argued that about another 50 cm^{-3} grew into sizes effective as CCN.2 in the MBL. It is clear that the surface area (Fig. 10c, d) and mass of these aerosol are strongly influenced by their growth in the MBL. Growth in this region is driven by the surface source of DMS and resulting accumulation of sulfate aerosol upon their surface (Clarke et al., 1996; Simpson, 2010). The amount of mass accumulated will depend upon variations in the source strength of DMS, wind speed,

photochemical processes, cloud presence, scavenging and the entrainment rate of the aerosol from the FT.

Assuming a near constant source strength of DMS and weak aerosol removal due to low cloud amount and precipitation in the PASE region, and other things being equal, then lower entrainment (weaker divergence) rates will lead to increased residence times and more uptake per particle (growth) than for higher entrainment. This also assumes that the in-cloud coagulation in these predominantly non-precipitating trade-wind clouds is small. The surface area plots and the size distribution changes evident in Fig. 10 show that most of the accumulated mass will occur on sizes larger than the Hoppel minimum. Out-of-cloud growth rates for sub-CCN.2 sizes are calculated to be on the order of 10 nm per day and much slower for larger sizes. In this region of low precipitation, the Hoppel minimum indicates most growth is likely dominated by in-cloud processes (Simpson, 2010) and by the uptake of sulfuric acid. Growth of sizes smaller than the Hoppel minimum into larger sizes is expected to be slow unless precipitation events scavenge most of the larger sizes. However, when combustion layers are entrained from above the inversion (e.g. Fig. 12) they contribute sizes that can fill in the Hoppel minimum. Entrainment is expected to be near cloud top in the BuL where they can readily activate and participate in heterogeneous growth processes. For estimated entrainment rates of about $0.5\,cm\,s^{-1}$ (Clarke et al., 1996; Conley et al., 2009), the air in the MBL can be diluted by a factor of two in about 2 days. Hence, this process can be an effective way to resupply CCN.2 directly into the Hoppel minimum size range in addition to growth of smaller sizes in the MBL. This increase of CCN in clean regions, where cloud properties are susceptible to small changes in aerosol, can have a disproportionate effects upon the regional energy balance (Yang et al., 2012) that is larger than from the first indirect effect (Twomey, 1974) alone.

FT aerosol were found to be strongly influenced by sources linked to ITCZ cloud outflow for CO < 63 ppbv and by combustion sources for CO > 63 ppbv. Trajectories for many elevated CO layers were from the Amazon after passing over the Andes mountains at about 5 km altitude. Mean subsidence rates of about $0.5\,cm\,s^{-1}$ over 10 000 km

Title Page

Abstract | Introduction

Conclusions | References

Tables | Figures

◄ | ►

◄ | ►

Back | Close

Full Screen / Esc

Printer-friendly Version

Interactive Discussion

brought these layers to the top of the TWI near Christmas Island after about 10 days or so. Hence, FT transport can provide a teleconnection between MBL aerosol over the central equatorial pacific and combustion aerosol ($CO > 63$ ppbv) convected aloft over South America. Alternately, the FT also provides a teleconnection to ITCZ aerosol out-flow ($CO < 63$ ppbv) often about 3000 km or more away. CCN entrained for the former higher CO cases can be 30 % higher than the latter low CO cases.

These sources and associated FT aerosol accounted for most of the CCN active in MBL clouds in this region and were entrained at sizes already effective as CCN. Concurrent flight-to-flight variations in these CCN at all three altitudes indicated the MBL concentrations were in quasi-equilibrium with the FT source on a scale of about 3 days. These observations suggest CCN in other regions may be similarly influenced via meteorologically preferred teleconnections in the FT to cloud scavenged aerosol from other distant upwind sources.

Virtually all MBL sulfate produced is accumulated on the larger entrained FT aerosol active as CCN in the MBL. No evidence for nucleation was found in the MBL and the smaller more volatile sizes nucleated in ITCZ cloud outflow appeared to be most rapidly depleted when mixed into the MBL. Hence, the so-called CLAW hypothesis (Charlson et al., 1987) is not effective in enhancing aerosol number active as CCN over this region at the time and season of PASE. However, the feedback mechanism between DMS and MBL CCN (Shaw et al., 1998) driven via cloud pumping of precursors aloft followed by nucleation in the FT remains a possibility when the influence of continental aerosol from long range transport is low.

Title Page

Abstract | Introduction

Conclusions | References

Tables | Figures

|◀ | ▶|

◀ | ▶

Back | Close

Full Screen / Esc

Printer-friendly Version

Interactive Discussion

References

Albrecht, B. A.: Aerosols, cloud microphysics, and fractional cloudiness, Science, 245, 1227–1230, doi:10.1126/science.245.4923.1227, 1989. 1281

Andreae, M. O.: Correlation between cloud condensation nuclei concentration and aerosol optical thickness in remote and polluted regions, Atmos. Chem. Phys., 9, 543–556, doi:10.5194/acp-9-543-2009, 2009. 1281

Andreae, M. O., Artaxo, P., Fischer, H., Freitas, S. R., Grégoire, J. M., Hansel, A., Hoor, P., Kormann, R., Krejci, R., Lange, L., Lelieveld, J., Lindinger, W., Longo, K., Peters, W., de Reus, M., Scheeren, B., Silva Dias, M. A. F., Ström, J., van Velthofen, P. F. J., and Williams, J.: Transport of biomass burning smoke to the upper troposphere by deep convection in the equatorial region, Geophys. Res. Lett., 28, 951–954, doi:10.1029/2000GL012391, 2001. 1303

Andreae, M. O., Rosenfeld, D., Artaxo, P., Costa, A. A., Frank, G. P., Longo, K. M., and Silva-Dias, M. A. F.: Smoking rain clouds over the Amazon, Science, 303, 1337–1342, doi:10.1126/science.1092779, 2004. 1303

Andronache, C., Grönholm, T., Laakso, L., Phillips, V., and Venäläinen, A.: Scavenging of ultrafine particles by rainfall at a boreal site: observations and model estimations, Atmos. Chem. Phys., 6, 4739–4754, doi:10.5194/acp-6-4739-2006, 2006. 1305

Bandy, A. R., Thornton, D. C., Blomquist, B. W., Chen, S., Wade, T., Ianni, J., Mitchell, G. M., and Nadler, W.: Chemistry of dimethyl sulfide in the equatorial Pacific atmosphere, Geophys. Res. Lett., 23, 741–744, doi:10.1029/96GL00779, 1996. 1282

Bandy, A., Faloona, I. C., Blomquist, B. W., Huebert, B. J., Clarke, A. D., Howell, S. G., Mauldin, R. L., Cantrell, C. A., Hudson, J. G., Heikes, B. G., Merrill, J. T., Wang, Y., O'Sullivan, D. W., Nadler, W., and Davis, D. D.: Pacific Atmospheric Sulfur Experiment (PASE): dynamics and chemistry of the South Pacific tropical trade wind regime, J. Atmos. Chem., 68, 5–25, doi:10.1007/s10874-012-9215-8, 2012. 1282

Browell, E. V., Fenn, M. A., Butler, C. F., Grant, W. B., Ismail, S., Ferrare, R. A., Kooi, S. A., Brackett, V. G., Clayton, M. B., Avery, M. A., Barrick, J. D. W., Fuelberg, H. E., Maloney, J. C., Newell, R. E., Zhu, Y., Mahoney, M. J., Anderson, B. E., Blake, D. R., Brune, W. H., Heikes, B. G., Sachse, G. W., Singh, H. B., and Talbot, R. W.: Large-scale air mass characteristics observed over the remote tropical Pacific Ocean during March–April 1999: results from

Title Page

Abstract | Introduction

Conclusions | References

Tables | Figures

◄ | ►

◄ | ►

Back | Close

Full Screen / Esc

Printer-friendly Version

Interactive Discussion

PEM-Tropics B field experiment, J. Geophys. Res., 108, 8805, doi:10.1029/2002JD003290, 2001. 1283

Charlson, R. J., Lovelockl, J. E., Andreaei, M. O., and Warren, S. G.: Oceanic phytoplankton, atmospheric sulphur, cloud albedo and climate, Nature, 326, 655–661, doi:10.1038/326655a0, 1987. 1307

Chatfield, R. B. and Crutzen, P. J.: Are there interactions of iodine and sulfur species in marine air photochemistry, J. Geophys. Res., 95, 22319–22341, doi:10.1029/JD095iD13p22319, 1990. 1281

Clarke, A. D.: Atmospheric nuclei in the Pacific midtroposphere: their nature, concentration, and evolution, J. Geophys. Res., 98, 20633–20647, doi:10.1029/93JD00797, 1993. 1305

Clarke, A. D. and Kapustin, V. N.: Hemispheric aerosol vertical profiles: anthropogenic impacts on optical depth and cloud nuclei, Science, 329, 1488–1492, doi:10.1126/science.1188838, 2010. 1281, 1282, 1303

Clarke, A. D., Li, Z., and Litchy, M.: Aerosol dynamics in the equatorial Pacific marine boundary layer: microphysics, diurnal cycles and entrainment, Geophys. Res. Lett., 23, 733–736, doi:10.1029/96GL00778, 1996. 1283, 1291, 1305, 1306

Clarke, A. D., Varner, J. L., Eisele, F., Mauldin, R. L., Tanner, D., and Litchy, M.: Particle production in the remote marine atmosphere: cloud outflow and subsidence during ACE 1, J. Geophys. Res., 103, 16397–16409, doi:10.1029/97JD02987, 1998a. 1281, 1287

Clarke, A. D., Davis, D., Kapustin, V. N., Eisele, F., Chen, G., Paluch, I., Lenschow, D., Bandy, A. R., Thornton, D., Moore, K., L. Mauldin, Tanner, D., Litchy, M., Carroll, M. A., Collins, J., and Albercook, G.: Particle nucleation in the tropical boundary layer and its coupling to marine sulfur sources, Science, 282, 89–92, doi:10.1126/science.282.5386.89, 1998b. 1281

Clarke, A. D., Kapustin, V. N., Eisele, F. L., Weber, R. J., and McMurry, P. H.: Particle production near marine clouds: sulfuric acid and predictions from classical binary nucleation, Geophys. Res. Lett., 26, 2425–2428, doi:10.1029/1999GL900438, 1999a. 1286

Clarke, A. D., Eisele, F., Kapustin, V. N., Moore, K., Tanner, D., Mauldin, L., Litchy, M., Lienert, B., Carroll, M. A., and Albercook, G.: Nucleation in the equatorial free troposphere: favorable environments during PEM-Tropics, J. Geophys. Res., 104, 5735–5744, doi:10.1029/98JD02303, 1999b. 1287, 1289, 1304

Clarke, A. D., Shinozuka, Y., Kapustin, V. N., Howell, S. G., Huebert, B., Doherty, S., Anderson, T., Covert, D., Anderson, J., Hua, X., Moore II, K. G., McNaughton, C., Carmichael, G.,

and Weber, R.: Size distributions and mixtures of dust and black carbon aerosol in Asian outflow: physiochemistry and optical properties, J. Geophys. Res., 109, D15S09, doi:10.1029/2003JD004378, 2004. 1284

Clarke, A. D., Owens, S. R., and Zhou, J.: An ultrafine sea-salt flux from breaking waves: implications for cloud condensation nuclei in the remote marine atmosphere, J. Geophys. Res., 111, D06202, doi:10.1029/2005JD006565, 2006. 1299

Conley, S. A., Faloona, I., Miller, G. H., Lenschow, D. H., Blomquist, B., and Bandy, A.: Closing the dimethyl sulfide budget in the tropical marine boundary layer during the Pacific Atmospheric Sulfur Experiment, Atmos. Chem. Phys., 9, 8745–8756, doi:10.5194/acp-9-8745-2009, 2009. 1291, 1306

Conley, S. A., Faloona, I. C., Lenschow, D. H., Campos, T., Heizer, C., Weinheimer, A., Cantrell, C. A., Mauldin III, R. L., Hornbrook, R. S., Pollack, I., and Bandy, A.: A complete dynamical ozone budget measured in the tropical marine boundary layer during PASE, J. Atmos. Chem., 68, 55–70, doi:10.1007/s10874-011-9195-0, 2011. 1286

Draxler, R. R.: HYSPLIT4 user's guide, NOAA Tech. Memo ERL ARL-230, NOAA Air Resources Laboratory, Silver Spring, MD, available at: http://www.arl.noaa.gov/documents/reports/hysplit_user_guide.pdf, 1999. 1289

Draxler, R. R. and Hess, G. D.: Description of the HYSPLIT_4 modeling system, NOAA Tech. Memo ERL ARL-224, NOAA Air Resources Laboratory, Silver Spring, MD, 24 pp., available at: http://arlsun.arlhq.noaa.gov/documents/reports/arl-224.pdf, 1997. 1289

Draxler, R. R. and Hess, G. D.: An overview of the HYSPLIT_4 modeling system of trajectories, dispersion, and deposition, available at: http://134.178.63.141/amm/docs/1998/draxler.pdf, Aust. Meteor. Mag., 47, 295–308, 1998. 1289

Faloona, I., Conley, S. A., Blomquist, B., Clarke, A. D., Kapustin, V. N., Howell, S. G., Lenschow, D. H., and Bandy, A. R.: Sulfur dioxide in the tropical marine boundary layer: dry deposition and heterogeneous oxidation observed during the Pacific Atmospheric Sulfur Experiment, J. Atmos. Chem., 63, 13–32, doi:10.1007/s10874-010-9155-0, 2009. 1282

Gunthe, S. S., King, S. M., Rose, D., Chen, Q., Roldin, P., Farmer, D. K., Jimenez, J. L., Artaxo, P., Andreae, M. O., Martin, S. T., and Pöschl, U.: Cloud condensation nuclei in pristine tropical rainforest air of Amazonia: size-resolved measurements and modeling of atmospheric aerosol composition and CCN activity, Atmos. Chem. Phys., 9, 7551–7575, doi:10.5194/acp-9-7551-2009, 2009. 1304

CCN in the Equatorial Pacific boundary layer

A. D. Clarke et al.

Title Page

Abstract | Introduction

Conclusions | References

Tables | Figures

◄◄ | ►►

◄ | ►

Back | Close

Full Screen / Esc

Printer-friendly Version

Interactive Discussion

Hegg, D. A., Hobbs, P. V., Ferek, R. J., and Waggoner, A. P.: Measurements of some aerosol properties relevant to radiative forcing on the east coast of the United States, J. Appl. Meteor., 1995, 2306–2315, doi:10.1175/1520-0450(1995)034<2306:MOSAPR>2.0.CO;2, 34. 1281

Hoell, J. M., Davis, D. D., Liu, S. C., Newell, R., Shipham, M., Akimoto, H., McNeal, R. J., Bendura, R. J., and Drewry, J. W.: Pacific exploratory Mission-West A (PEM-West A): September October 1991, J. Geophys. Res., 101, 1641–1653, doi:10.1029/95JD00622, 1996. 1281

Hoppel, W. A., Frick, G. M., Fitzgerald, J. W., and Larson, R. E.: Marine boundary layer measurements of new particle formation and the effects nonprecipitating clouds have on aerosol size distribution, J. Geophys. Res., 99, 14443–14459, doi:10.1029/94JD00797, 1994. 1284

Hudson, J. G. and Noble, S.: CCN and cloud droplet concentrations at a remote ocean site, Geophys. Res. Lett., 36, L13812, doi:10.1029/2009GL038465, 2009. 1283, 1284

Hudson, J. G., Jha, V., and Noble, S.: Drizzle correlations with giant nuclei, Geophys. Res. Lett., 38, L05808, doi:10.1029/2010GL046207, 2011. 1284, 1296, 1300

Huebert, B. J., Wylie, D. J., Zhuang, L., and Heath, J. A.: Production and loss of methanesulfonate and non-sea salt sulfate in the equatorial Pacific marine boundary layer, Geophys. Res. Lett., 23, 737–740, doi:10.1029/96GL00777, 1996. 1283, 1291

Jensen, J. B. and Charlson, R. J.: On the efficiency of nucleation scavenging, Tellus B, 36, 367–375, doi:10.1111/j.1600-0889.1984.tb00255.x, 1984. 1281

Kaufman, Y. J., Tanre, D., Holben, B. N., Mattoo, S., Remer, L. A., Eck, T. F., Vaughan, J., and Chatenet, B.: Aerosol radiative impact on spectral solar flux at the surface, derived from principal-plane sky measurements, J. Atmos. Sci., 59, 635–646, doi:10.1175/1520-0469(2002)059<0635:ARIOSS>2.0.CO;2, 2002. 1281

Kim, J. H. and Newchurch, M. J.: Climatology and trends of tropospheric ozone over the eastern Pacific Ocean: the influences of biomass burning and tropospheric dynamics, Geophys. Res. Lett., 23, 3723–3726, doi:10.1029/96GL03615, 1996. 1283

Martin, S. T., Andreae, M. O., Althausen, D., Artaxo, P., Baars, H., Borrmann, S., Chen, Q., Farmer, D. K., Guenther, A., Gunthe, S. S., Jimenez, J. L., Karl, T., Longo, K., Manzi, A., Müller, T., Pauliquevis, T., Petters, M. D., Prenni, A. J., Pöschl, U., Rizzo, L. V., Schneider, J., Smith, J. N., Swietlicki, E., Tota, J., Wang, J., Wiedensohler, A., and Zorn, S. R.: An overview of the Amazonian Aerosol Characterization Experiment 2008 (AMAZE-08), Atmos. Chem. Phys., 10, 11415–11438, doi:10.5194/acp-10-11415-2010, 2010. 1305

Merikanto, J., Spracklen, D. V., Mann, G. W., Pickering, S. J., and Carslaw, K. S.: Impact of nucleation on global CCN, Atmos. Chem. Phys., 9, 8601–8616, doi:10.5194/acp-9-8601-2009, 2009. 1304, 1305

Moore II, K. G., Clarke, A. D., Kapustin, V. N., and Howell, S. G.: Long-range transport of continental plumes over the Pacific Basin: aerosol physiochemistry and optical properties during PEM-Tropics A and B, J. Geophys. Res., 108, 8236, doi:10.1029/2001JD001451, 2003. 1283, 1303, 1304

Negri, A. J., Anagnostou, E. N., and Adler, R. F.: A 10-yr climatology of Amazonian rainfall derived from passive microwave satellite observations, J. Appl. Meteor., 39, 42–56, doi:10.1175/1520-0450(2000)039<0042:AYCOAR>2.0.CO;2, 2000. 1291

Rissler, J., Vestin, A., Swietlicki, E., Fisch, G., Zhou, J., Artaxo, P., and Andreae, M. O.: Size distribution and hygroscopic properties of aerosol particles from dry-season biomass burning in Amazonia, Atmos. Chem. Phys., 6, 471–491, doi:10.5194/acp-6-471-2006, 2006. 1303

Schmeissner, T., Krejci, R., Ström, J., Birmili, W., Wiedensohler, A., Hochschild, G., Gross, J., Hoffmann, P., and Calderon, S.: Analysis of number size distributions of tropical free tropospheric aerosol particles observed at Pico Espejo (4765 m a.s.l.), Venezuela, Atmos. Chem. Phys., 11, 3319–3332, doi:10.5194/acp-11-3319-2011, 2011. 1303

Shank, L. M., Howell, S., Clarke, A. D., Freitag, S., Brekhovskikh, V., Kapustin, V., McNaughton, C., Campos, T., and Wood, R.: Organic matter and non-refractory aerosol over the remote Southeast Pacific: oceanic and combustion sources, Atmos. Chem. Phys., 12, 557–576, doi:10.5194/acp-12-557-2012, 2012. 1284

Shaw, G. E., Benner, R. L., Cantrell, W., and Clarke, A. D.: On the regulation of climate: a sulfate particle feedback loop involving deep convection, Climatic Change, 39, 23–33, doi:10.1023/A:1005341506115, 1998. 1307

Simpson, R. M. C.: Mechanisms of sulfate production in the remote equatorial Pacific marine boundary layer, Master's thesis, University of Hawai'i at Manoa, available at: http://www.soest.hawaii.edu/oceanography/masters/Simpson.pdf, 2010. 1283, 1286, 1295, 1297, 1298, 1301, 1302, 1305, 1306

Soto-García, L. L., Andreae, M. O., Andreae, T. W., Artaxo, P., Maenhaut, W., Kirchstetter, T., Novakov, T., Chow, J. C., and Mayol-Bracero, O. L.: Evaluation of the carbon content of aerosols from the burning of biomass in the Brazilian Amazon using thermal, optical and thermal-optical analysis methods, Atmos. Chem. Phys., 11, 4425–4444, doi:10.5194/acp-11-4425-2011, 2011. 1303, 1304

Staudt, A. C., Jacob, D. J., Logan, J. A., Bachiochi, D., Krishnamurti, T. N., and Sachse, G. W.: Continental sources, transoceanic transport, and interhemispheric exchange of carbon monoxide over the Pacific, J. Geophys. Res., 106, 32571–32590, doi:10.1029/2001JD900078, 2001. 1285, 1293

Thornberry, T., Froyd, K. D., Murphy, D. M., Thomson, D. S., Anderson, B. E., Thornhill, K. L., and Winstead, E. L.: Persistence of organic carbon in heated aerosol residuals measured during Tropical Composition Cloud and Climate Coupling (TC4), J. Geophys. Res., 115, D00J02, doi:10.1029/2009JD012721, 2010. 1282

Twomey, S.: Pollution and the planetary albedo, Atmos. Environ., 8, 1251–1256, doi:10.1016/0004-6981(74)90004-3, 1974. 1281, 1306

Yang, M., Blomquist, B. W., Fairall, C. W., Archer, S. D., and Huebert, B. J.: Air-sea exchange of dimethylsulfide in the Southern Ocean: measurements from SO GasEx compared to temperate and tropical regions, J. Geophys. Res., 116, C00F05, doi:10.1029/2010JC006526, 2011. 1295

Yang, Q., W. I. Gustafson Jr., Fast, J. D., Wang, H., Easter, R. C., Morrison, H., Lee, Y.-N., Chapman, E. G., Spak, S. N., and Mena-Carrasco, M. A.: Assessing regional scale predictions of aerosols, marine stratocumulus, and their interactions during VOCALS-REx using WRF-Chem, Atmos. Chem. Phys., 11, 11951–11975, doi:10.5194/acp-11-11951-2011, 2011. 1306

Title Page

Abstract | Introduction

Conclusions | References

Tables | Figures

◄ | ►

◄ | ►

Back | Close

Full Screen / Esc

Printer-friendly Version

Interactive Discussion

Table 1. Mean concentrations of key parameters in lower BL, BuL and FT < 3 km.

	BL	BuL	FT < 3 km	BL minus FT < 3 km	BuL minus FT < 3 km
CO (ppbv)	63	63	61	2	2
O_3 (pbbv)	18	20	25	−7	−5
SO_2 (pptv)	52	38	37	15	2
DMS (pptv)	71	36	5	66	31
CNhot (cm^{-3})	253	212	158	95	55
CNvol (cm^{-3})	185	217	375	−191	−158
CNtot (cm^{-3})	438	429	533	−95	−104
CCN.04 (cm^{-3})	63	56	24	39	32
CCN.2 (cm^{-3})	192	182	125	67	57
CCN.4 (cm^{-3})	241	235	187	54	48
ScatTot (Mm^{-1})	31	15	2	29	13
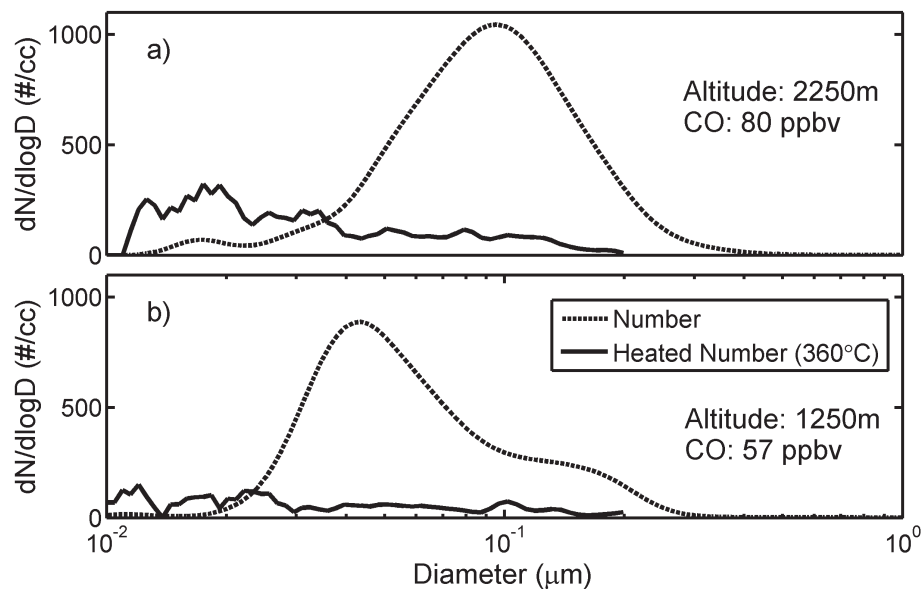
Fig. 1. Examples of DMA distributions in the FT from RF08 for a low CO layer and high CO layer before (dotted) and after heating to 360 ˚C (solid).
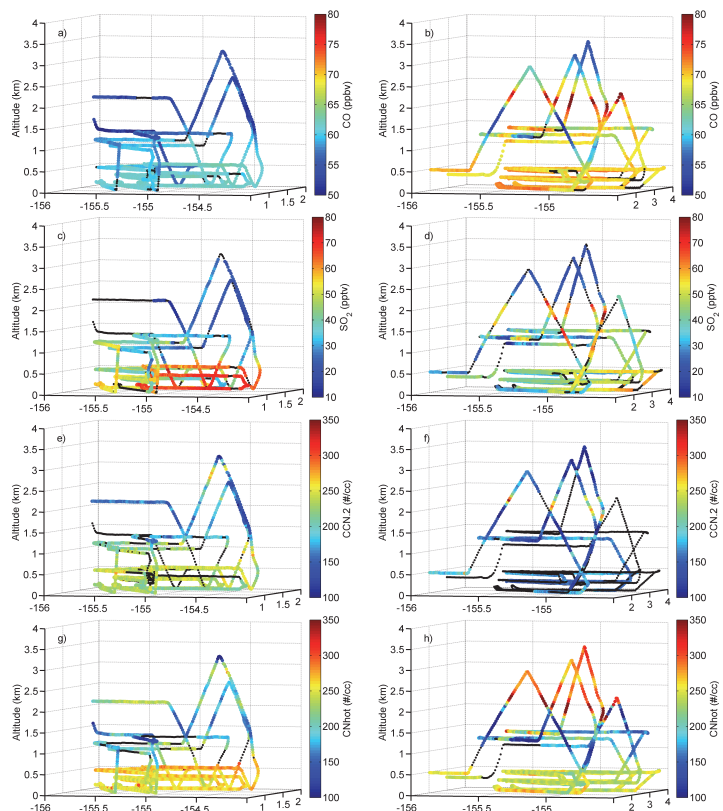
Fig. 2. Examples of a low CO (RF03, 13 August, left column) and higher CO (RF08, 25 August right column) flights with selected data color coded along path as indicated. Black line indicates no data available.

CCN in the Equatorial Pacific boundary layer

A. D. Clarke et al.

Title Page

Abstract | Introduction

Conclusions | References

Tables | Figures

◀ | ▶

◀ | ▶

Back | Close

Full Screen / Esc

Printer-friendly Version

Interactive Discussion
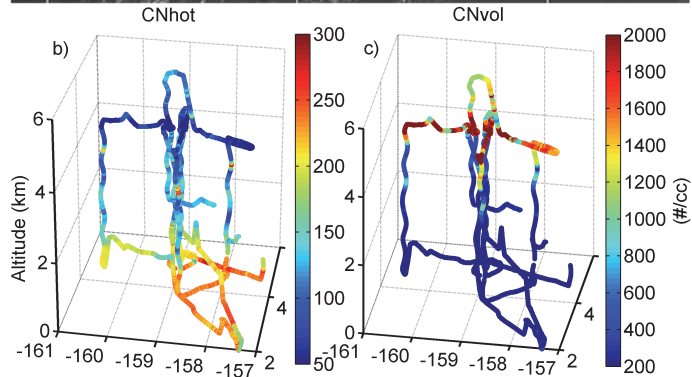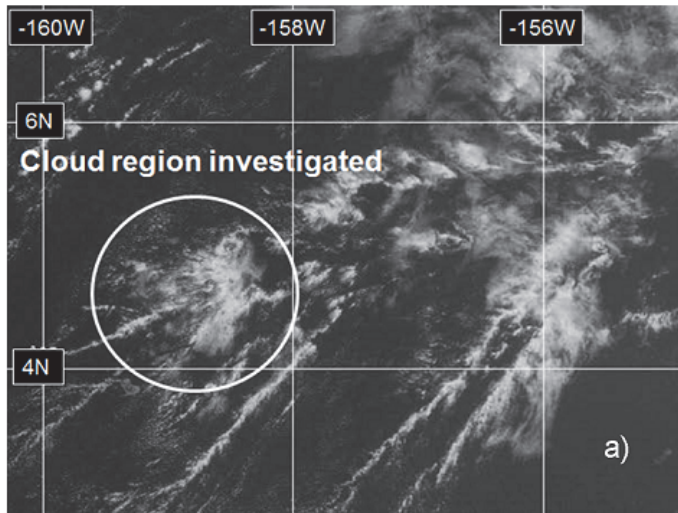
Fig. 3. OES image **(a)** showing cloud targeted for RF04 study. Flight path plots (bottom) color coded with CNhot **(b)** and CNvol **(c)**. Horizontal legs to west, south and east flown in outflow layers at 4.3 km show marked depletions of CNhot and strong enhancement of CNvol relative to MBL.
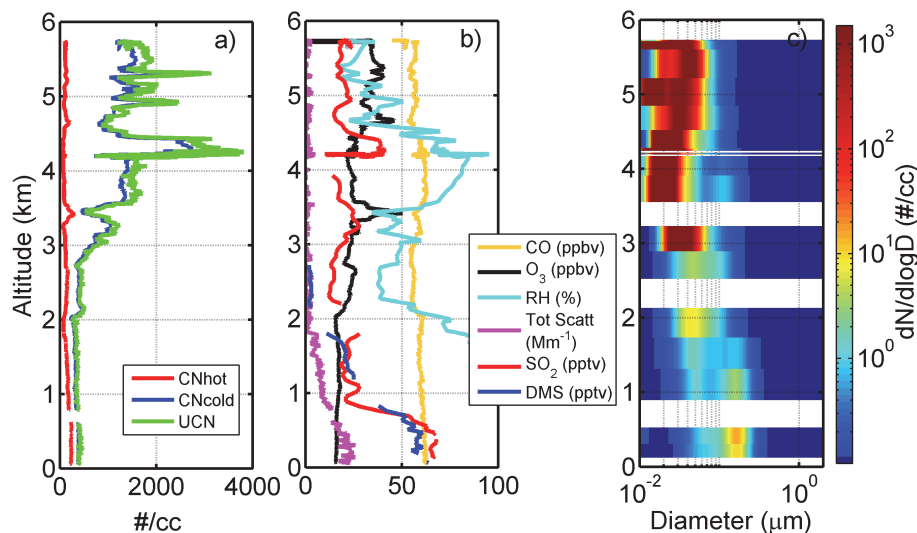
Fig. 4. Example profile for RF04 cloud study. Left panel shows CNhot generally decreases with altitude and is anti-correlated with CNcold and UCN. Middle panel shows DMS maximum near surface is depleted above inversion, as is total aerosol light scattering. Enhanced outflow between 3600–4400 m is associated with higher RH and shows increased nucleation. Reduced CNhot is most evident near 4300 m where SO_2 and CO are close to surface values (see text for details).
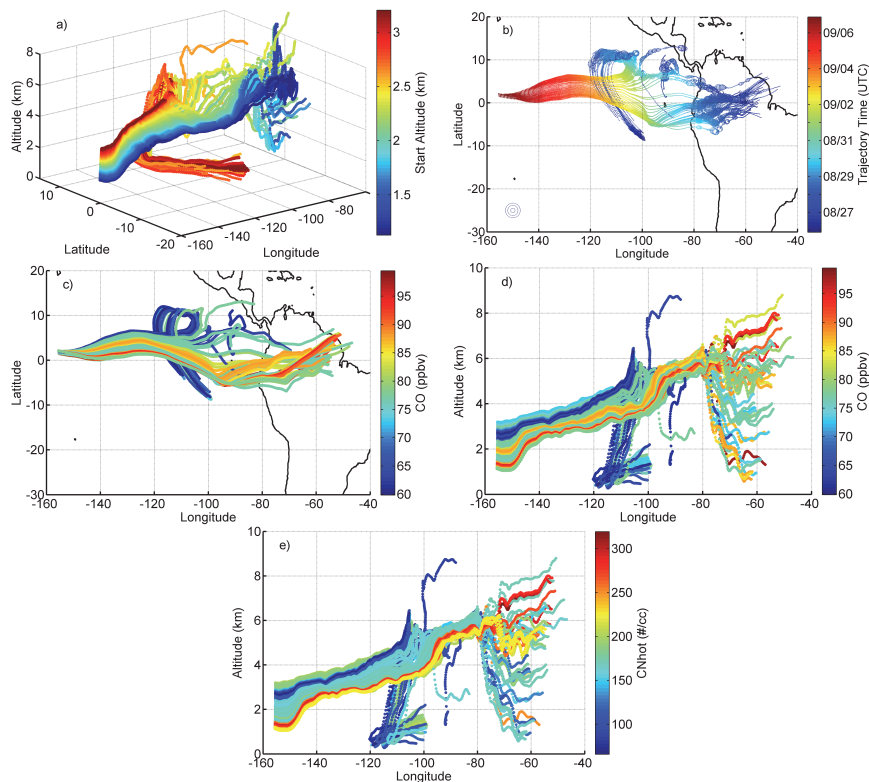
Fig. 5. Back trajectories for RF14 color coded with **(a)** aircraft start altitude for 3-D trajectories, **(b)** date on latitude-longitude projection with HYSPLIT precipitation expressed in marker size. The blue circles in the lower left corner exemplify precipitation intensities of $1/5/10\,\mathrm{mm\,h}^{-1}$. Plot **(c)** shows measured CO on latitude-longitude projection, **(d)** CO on vertical projection and **(e)** CNhot on vertical projection. Note that N/S distances are magnified by a factor of 5 relative to E/W.

Title Page

Abstract | Introduction

Conclusions | References

Tables | Figures

◀◀ | ▶▶

◀ | ▶

Back | Close

Full Screen / Esc

Printer-friendly Version

Interactive Discussion
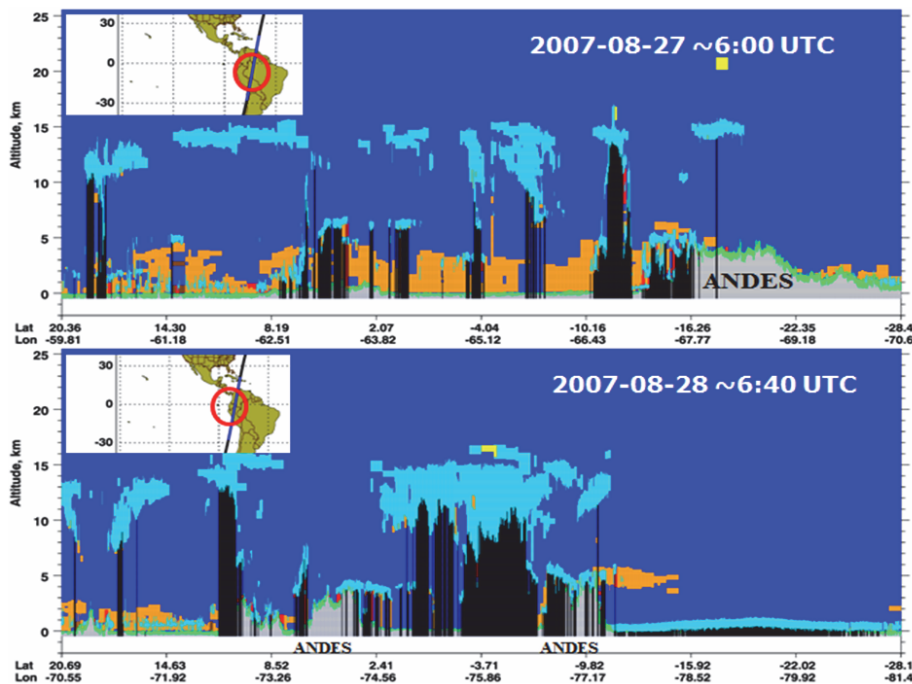
Fig. 6. CALIPSO data for indicated times and locations associated with back trajectories to these locations shown in Fig. 5. Strong pollution from biomass burning fills the Amazon basin (top-orange). Deep convection in the region of maximum Amazonian precipitation is evident in Ecuador east of the Andes near 3.71° S as a precipitation-attenuated signal (black) below clouds (light blue). Some cloud pumping and transport of aerosol (orange) over the Andes is also evident.
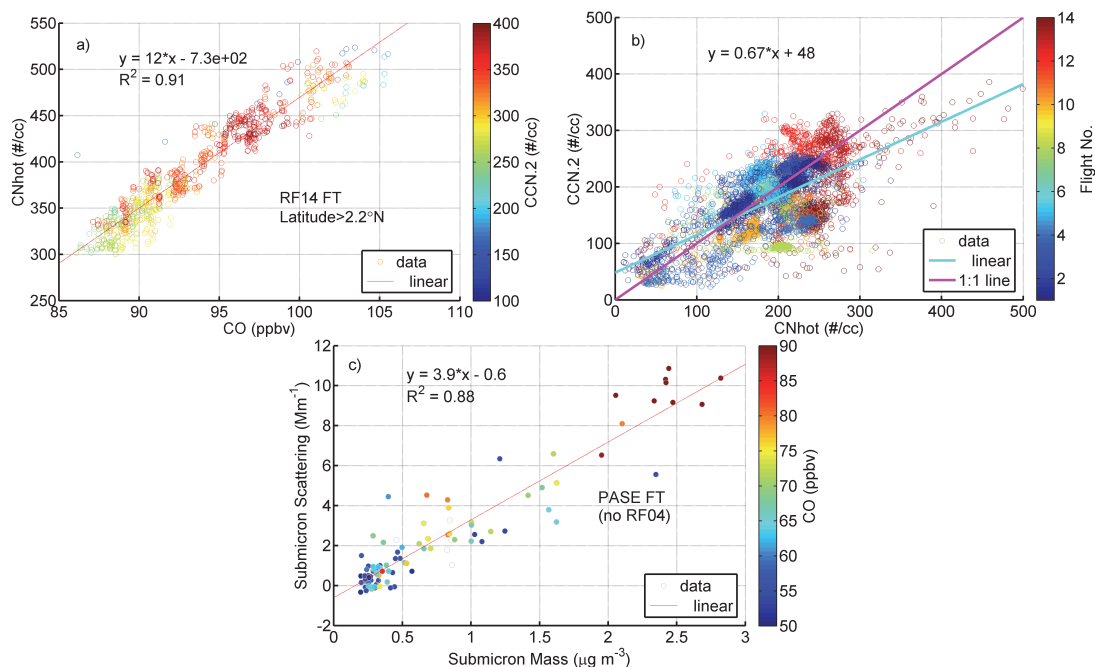
Fig. 7. (a) An example of typical correlation between CNhot and CO in an FT elevated CO layer colored with CCN.2; **(b)** the relation between CNhot and CCN.2 for all PASE flights colored with flight number; **(c)** submicrometer light scattering vs. submicrometer mass from the OPC above TWI colored with CO.
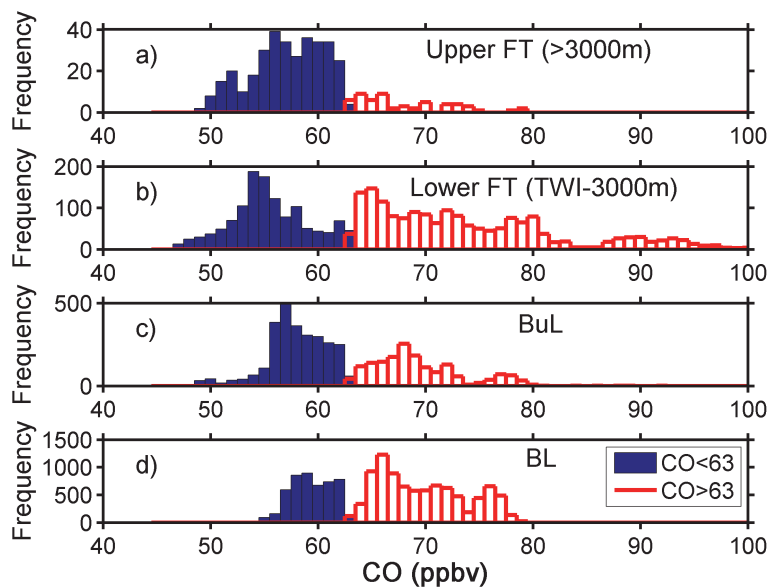
Fig. 8. Histograms of observed CO concentrations during PASE for indicated altitude ranges. A few measurements in the lower FT exceeded 100 ppbv but are not shown here for plot clarity.

Discussion Paper | Discussion Paper | Discussion Paper | Discussion Paper |

ACPD

13, 1279–1326, 2013

CCN in the Equatorial Pacific boundary layer

A. D. Clarke et al.

Title Page

Abstract · Introduction

Conclusions · References

Tables · Figures

◄ · ►

◄ · ►

Back · Close

Full Screen / Esc

Printer-friendly Version

Interactive Discussion
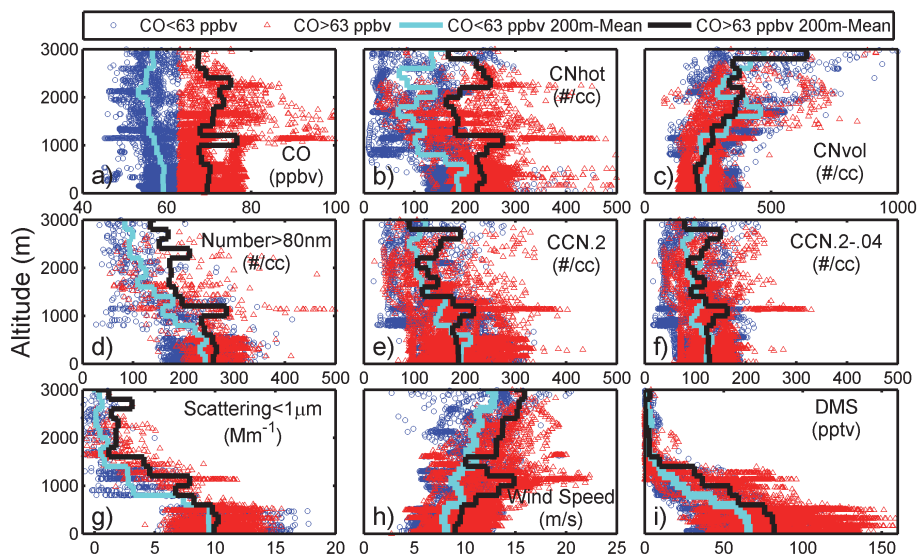
Fig. 9. Vertical profiles for diverse measurements for all PASE data when classified by CO values above (red) and below 63 ppbv (blue) as shown in **(a)** and discussed in Fig. 8.

Title Page

Abstract | Introduction

Conclusions | References

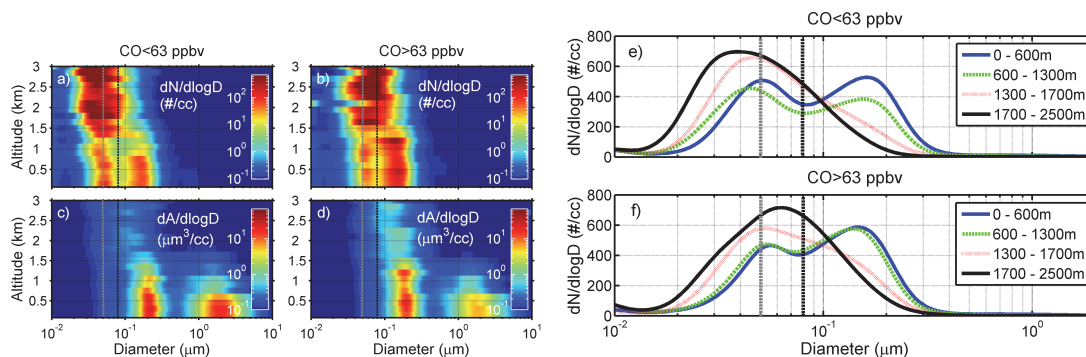Tables | Figures

|◄ | ►|

◄ | ►

Back | Close

Full Screen / Esc

Printer-friendly Version

Interactive Discussion

Fig. 10. (a–d) PASE mission averaged vertical profiles of size distributions color coded by number (upper) and area (lower) for low CO (left) and high CO (right) data. **(e–f)** mean size distributions for indicated altitude ranges stratified by CO. The black vertical line indicates the Hoppel minimum, the representative diameter above which particles are active CCN in typical clouds, while the vertical gray line approximates the start of the minimum, showing the smallest sizes at which activation occurs.
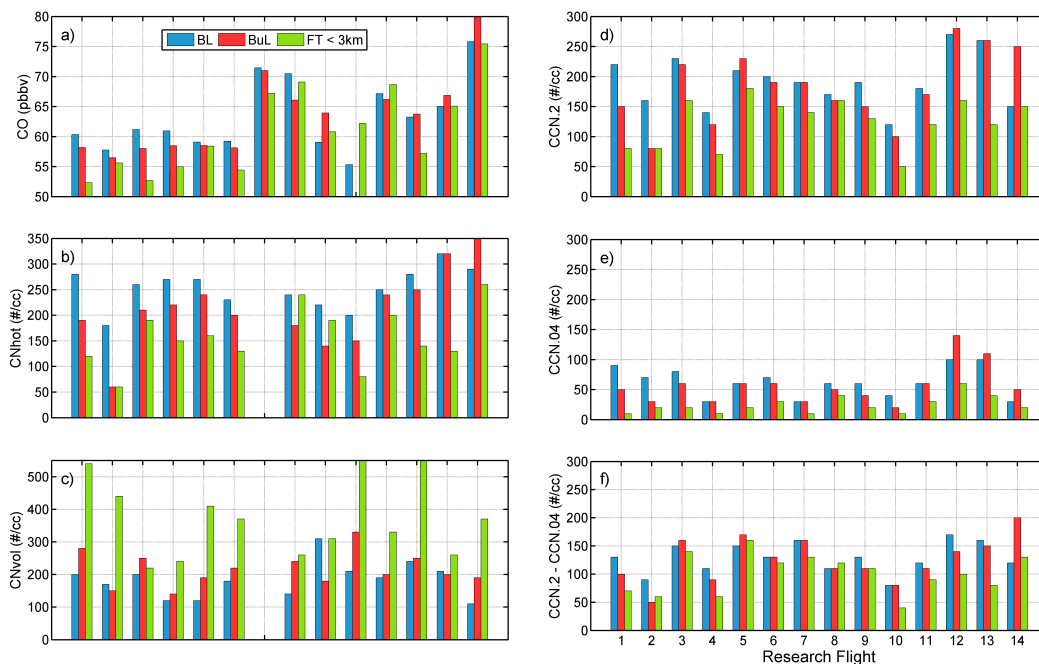
Fig. 11. Mean values over each flight for indicated PASE measurements in the surface mixed layer (BL), buffer layer (BuL) and in the FT < 3 km. See text for details.

Title Page

Abstract | Introduction

Conclusions | References

Tables | Figures

◄◄ | ►►

◄ | ►

Back | Close

Full Screen / Esc

Printer-friendly Version

Interactive Discussion
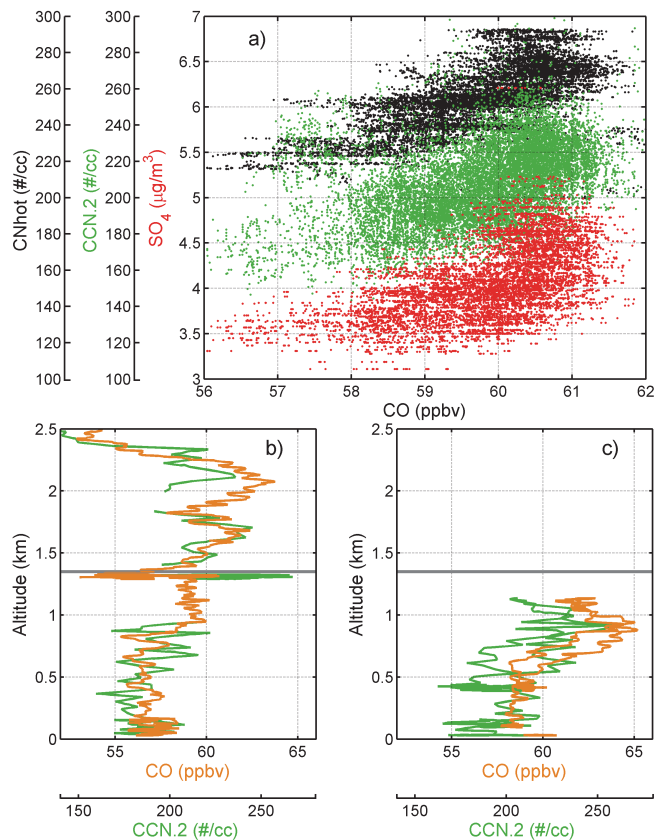
Fig. 12. (a) Trends in CNhot, CCN.2, and AMS sulfate vs. CO for level MBL legs in RF05; **(b–c)** profiles of CO and CCN.2 for RF05.